Article

# Search for standard model Higgs boson production in association with a W boson at CDF

CDF Collaboration

CLARK, Allan Geoffrey (Collab.), *et al*.

**Abstract**

We present a search for standard model Higgs boson production in association with a W boson in proton-antiproton collisions ($p\bar{p} \to W^{\pm}H \to \ell\nu b\bar{b}$) at a center of mass energy of 1.96 TeV. The search employs data collected with the CDF II detector which correspond to an integrated luminosity of approximately 1 $fb^{-1}$. We select events consistent with a signature of a single lepton ($e^{\pm}/\mu^{\pm}$), missing transverse energy, and two jets. Jets corresponding to bottom quarks are identified with a secondary vertex tagging method and a neural network filter technique. The observed number of events and the dijet mass distributions are consistent with the standard model background expectations, and we set 95% confidence level upper limits on the production cross section times branching ratio ranging from 3.9 to 1.3 pb for Higgs boson masses from 110 to 150 GeV/$c^2$, respectively.

Reference

CDF Collaboration, CLARK, Allan Geoffrey (Collab.), *et al*. Search for standard model Higgs boson production in association with a W boson at CDF. *Physical review. D. Particles, fields, gravitation, and cosmology*, 2008, vol. 78, no. 03, p. 032008

DOI : 10.1103/PhysRevD.78.032008

# Search for standard model Higgs boson production in association with a *W* boson at CDF

T. Aaltonen,[24] J. Adelman,[14] T. Akimoto,[55] M. G. Albrow,[18] B. Álvarez González,[12] S. Amerio,[43,a] D. Amidei,[35] A. Anastassov,[38] A. Annovi,[20] J. Antos,[15] G. Apollinari,[18] A. Apresyan,[48] T. Arisawa,[57] A. Artikov,[16] W. Ashmanskas,[18] A. Attal,[4] A. Aurisano,[53] F. Azfar,[42] P. Azzurri,[46,b] W. Badgett,[18] A. Barbaro-Galtieri,[29] V. E. Barnes,[48] B. A. Barnett,[26] V. Bartsch,[31] G. Bauer,[33] P.-H. Beauchemin,[34] F. Bedeschi,[46] P. Bednar,[15] D. Beecher,[31] S. Behari,[26] G. Bellettini,[46,c] J. Bellinger,[59] D. Benjamin,[17] A. Beretvas,[18] J. Beringer,[29] A. Bhatti,[50] M. Binkley,[18] D. Bisello,[43,a] I. Bizjak,[31] R. E. Blair,[2] C. Blocker,[7] B. Blumenfeld,[26] A. Bocci,[17] A. Bodek,[49] V. Boisvert,[49] G. Bolla,[48] D. Bortoletto,[48] J. Boudreau,[47] A. Boveia,[11] B. Brau,[11] A. Bridgeman,[25] L. Brigliadori,[43] C. Bromberg,[36] E. Brubaker,[14] J. Budagov,[16] H. S. Budd,[49] S. Budd,[25] K. Burkett,[18] G. Busetto,[43,a] P. Bussey,[22] A. Buzatu,[34] K. L. Byrum,[2] S. Cabrera,[17,d] C. Calancha,[32] M. Campanelli,[36] M. Campbell,[35] F. Canelli,[18] A. Canepa,[45] D. Carlsmith,[59] R. Carosi,[46] S. Carrillo,[19,e] S. Carron,[34] B. Casal,[12] M. Casarsa,[18] A. Castro,[6,f] P. Catastini,[46,g] D. Cauz,[54,h] V. Cavaliere,[46,g] M. Cavalli-Sforza,[4] A. Cerri,[29] L. Cerrito,[31,i] S. H. Chang,[28] Y. C. Chen,[1] M. Chertok,[8] G. Chiarelli,[46] G. Chlachidze,[18] F. Chlebana,[18] K. Cho,[28] D. Chokheli,[16] J. P. Chou,[23] G. Choudalakis,[33] S. H. Chuang,[52] K. Chung,[13] W. H. Chung,[59] Y. S. Chung,[49] C. I. Ciobanu,[44] M. A. Ciocci,[46,g] A. Clark,[21] D. Clark,[7] G. Compostella,[43] M. E. Convery,[18] J. Conway,[8] K. Copic,[35] M. Cordelli,[20] G. Cortiana,[43,a] D. J. Cox,[8] F. Crescioli,[46,c] C. Cuenca Almenar,[8,d] J. Cuevas,[12,j] R. Culbertson,[18] J. C. Cully,[35] M. Datta,[18] T. Davies,[22] P. de Barbaro,[49] S. De Cecco,[51] A. Deisher,[29] G. De Lorenzo,[4] M. Dell'Orso,[46,c] C. Deluca,[4] L. Demortier,[50] J. Deng,[17] M. Deninno,[6,f] P. F. Derwent,[18] G. P. di Giovanni,[44] C. Dionisi,[51,k] B. Di Ruzza,[54,h] J. R. Dittmann,[5] M. D'Onofrio,[4] S. Donati,[46,c] P. Dong,[9] J. Donini,[43] T. Dorigo,[52] S. Dube,[52] J. Efron,[39] A. Elagin,[53] R. Erbacher,[8] D. Errede,[25] S. Errede,[25] R. Eusebi,[18] H. C. Fang,[29] S. Farrington,[42] W. T. Fedorko,[14] R. G. Feild,[60] M. Feindt,[27] J. P. Fernandez,[32] C. Ferrazza,[46,b] R. Field,[19] G. Flanagan,[48] R. Forrest,[8] M. Franklin,[23] J. C. Freeman,[18] I. Furic,[19] M. Gallinaro,[51] J. Galyardt,[13] F. Garberson,[11] J. E. Garcia,[46] A. F. Garfinkel,[48] K. Genser,[18] H. Gerberich,[25] D. Gerdes,[35] A. Gessler,[27] S. Giagu,[51,k] V. Giakoumopoulou,[3] P. Giannetti,[46] K. Gibson,[47] J. L. Gimmell,[49] C. M. Ginsburg,[18] N. Giokaris,[3] M. Giordani,[54,h] P. Giromini,[20] M. Giunta,[46,c] G. Giurgiu,[26] V. Glagolev,[16] D. Glenzinski,[18] M. Gold,[37] N. Goldschmidt,[19] A. Golossanov,[18] G. Gomez,[12] G. Gomez-Ceballos,[33] M. Goncharov,[53] O. González,[32] I. Gorelov,[37] A. T. Goshaw,[17] K. Goulianos,[50] A. Gresele,[43,a] S. Grinstein,[23] C. Grosso-Pilcher,[14] R. C. Group,[18] U. Grundler,[25] J. Guimaraes da Costa,[23] Z. Gunay-Unalan,[36] C. Haber,[29] K. Hahn,[33] S. R. Hahn,[18] E. Halkiadakis,[52] B.-Y. Han,[49] J. Y. Han,[49] R. Handler,[59] F. Happacher,[20] K. Hara,[55] D. Hare,[52] M. Hare,[56] S. Harper,[42] R. F. Harr,[58] R. M. Harris,[18] M. Hartz,[47] K. Hatakeyama,[50] J. Hauser,[9] C. Hays,[42] M. Heck,[27] A. Heijboer,[45] B. Heinemann,[29] J. Heinrich,[45] C. Henderson,[33] M. Herndon,[59] J. Heuser,[27] S. Hewamanage,[5] D. Hidas,[17] C. S. Hill,[11,l] D. Hirschbuehl,[27] A. Hocker,[18] S. Hou,[1] M. Houlden,[30] S.-C. Hsu,[10] B. T. Huffman,[42] R. E. Hughes,[39] U. Husemann,[60] J. Huston,[36] J. Incandela,[11] G. Introzzi,[46] M. Iori,[51,k] A. Ivanov,[8] E. James,[18] B. Jayatilaka,[17] E. J. Jeon,[28] S. Jindariani,[18] W. Johnson,[8] M. Jones,[48] K. K. Joo,[28] S. Y. Jun,[13] J. E. Jung,[28] T. R. Junk,[18] T. Kamon,[53] D. Kar,[19] P. E. Karchin,[58] Y. Kato,[41] R. Kephart,[18] J. Keung,[45] V. Khotilovich,[53] B. Kilminster,[39] D. H. Kim,[28] H. S. Kim,[28] J. E. Kim,[28] M. J. Kim,[20] S. B. Kim,[28] S. H. Kim,[55] Y. K. Kim,[14] N. Kimura,[55] L. Kirsch,[7] S. Klimenko,[19] B. Knuteson,[33] B. R. Ko,[17] S. A. Koay,[11] K. Kondo,[57] D. J. Kong,[28] J. Konigsberg,[19] A. Korytov,[19] A. V. Kotwal,[17] M. Kreps,[27] J. Kroll,[45] N. Krumnack,[5] M. Kruse,[17] V. Krutelyov,[11] T. Kubo,[55] T. Kuhr,[27] N. P. Kulkarni,[58] M. Kurata,[55] Y. Kusakabe,[57] S. Kwang,[14] A. T. Laasanen,[48] S. Lami,[46] S. Lammel,[18] M. Lancaster,[31] R. L. Lander,[8] K. Lannon,[39] A. Lath,[52] G. Latino,[46,g] I. Lazzizzera,[43,a] T. LeCompte,[2] E. Lee,[53] J. Lee,[28] Y. J. Lee,[28] S. W. Lee,[53,m] S. Leone,[46] S. Levy,[14] J. D. Lewis,[18] C. S. Lin,[29] J. Linacre,[42] M. Lindgren,[18] E. Lipeles,[10] A. Lister,[8] D. O. Litvintsev,[18] C. Liu,[47] T. Liu,[18] N. S. Lockyer,[45] A. Loginov,[60] M. Loreti,[43,a] L. Lovas,[15] R.-S. Lu,[1] D. Lucchesi,[43,a] J. Lueck,[27] C. Luci,[51,k] P. Lujan,[29] P. Lukens,[18] G. Lungu,[50] L. Lyons,[42] J. Lys,[29] R. Lysak,[15] E. Lytken,[48] P. Mack,[27] D. MacQueen,[34] R. Madrak,[18] K. Maeshima,[18] K. Makhoul,[33] T. Maki,[24] P. Maksimovic,[26] S. Malde,[42] S. Malik,[31] G. Manca,[30] A. Manousakis-Katsikakis,[3] F. Margaroli,[48] C. Marino,[27] C. P. Marino,[25] A. Martin,[60] V. Martin,[22,n] M. Martínez,[4] R. Martínez-Ballarín,[32] T. Maruyama,[55] P. Mastrandrea,[51,k] T. Masubuchi,[55] M. E. Mattson,[58] P. Mazzanti,[6] K. S. McFarland,[49] P. McIntyre,[53] R. McNulty,[30,o] A. Mehta,[30] P. Mehtala,[24] A. Menzione,[46] P. Merkel,[48] C. Mesropian,[50] T. Miao,[18] N. Miladinovic,[7] R. Miller,[36] C. Mills,[23] M. Milnik,[27] A. Mitra,[1] G. Mitselmakher,[19] H. Miyake,[55] N. Moggi,[6] C. S. Moon,[28] R. Moore,[18] M. J. Morello,[46,c] J. Morlok,[27] P. Movilla Fernandez,[18] J. Mülmenstädt,[29] A. Mukherjee,[18] Th. Muller,[27] R. Mumford,[26] P. Murat,[18] M. Mussini,[6,f] J. Nachtman,[18] Y. Nagai,[55] A. Nagano,[55] J. Naganoma,[57] K. Nakamura,[55] I. Nakano,[40] A. Napier,[56] V. Necula,[17] C. Neu,[45] M. S. Neubauer,[25] J. Nielsen,[29,f] L. Nodulman,[2] M. Norman,[10] O. Norniella,[25] E. Nurse,[31] L. Oakes,[42] S. H. Oh,[17] Y. D. Oh,[28] I. Oksuzian,[19] T. Okusawa,[41] R. Orava,[24] K. Osterberg,[24] S. Pagan Griso,[43,a]

 

C. Pagliarone,[46] E. Palencia,[18] V. Papadimitriou,[18] A. Papaikonomou,[27] A. A. Paramonov,[14] B. Parks,[39] S. Pashapour,[34] J. Patrick,[18] G. Pauletta,[54,h] M. Paulini,[13] C. Paus,[33] D. E. Pellett,[8] A. Penzo,[54] T. J. Phillips,[17] G. Piacentino,[46] E. Pianori,[45] L. Pinera,[19] K. Pitts,[25] C. Plager,[9] L. Pondrom,[59] O. Poukhov,[16] N. Pounder,[42] F. Prakoshyn,[16] A. Pronko,[18] J. Proudfoot,[2] F. Ptohos,[18,q] E. Pueschel,[13] G. Punzi,[46,c] J. Pursley,[59] J. Rademacker,[42,l] A. Rahaman,[47] V. Ramakrishnan,[59] N. Ranjan,[48] I. Redondo,[32] B. Reisert,[18] V. Rekovic,[37] P. Renton,[42] M. Rescigno,[51] S. Richter,[27] F. Rimondi,[6,f] L. Ristori,[46] A. Robson,[22] T. Rodrigo,[12] T. Rodriguez,[45] E. Rogers,[25] S. Rolli,[56] R. Roser,[18] M. Rossi,[54] R. Rossin,[11] P. Roy,[34] A. Ruiz,[12] J. Russ,[13] V. Rusu,[18] H. Saarikko,[24] A. Safonov,[53] W. K. Sakumoto,[49] O. Saltó,[4] L. Santi,[54,h] S. Sarkar,[51,k] L. Sartori,[46] K. Sato,[18] A. Savoy-Navarro,[44] T. Scheidle,[27] P. Schlabach,[18] A. Schmidt,[27] E. E. Schmidt,[18] M. A. Schmidt,[14] M. P. Schmidt,[60] M. Schmitt,[38] T. Schwarz,[8] L. Scodellaro,[12] A. L. Scott,[11] A. Scribano,[46,g] F. Scuri,[46] A. Sedov,[48] S. Seidel,[37] Y. Seiya,[41] A. Semenov,[16] L. Sexton-Kennedy,[18] A. Sfyrla,[21] S. Z. Shalhout,[58] T. Shears,[30] P. F. Shepard,[47] D. Sherman,[23] M. Shimojima,[55,r] M. Shochet,[14] Y. Shon,[59] I. Shreyber,[21] A. Sidoti,[46] P. Sinervo,[34] A. Sisakyan,[16] A. J. Slaughter,[18] J. Slaunwhite,[39] K. Sliwa,[56] J. R. Smith,[8] F. D. Snider,[18] R. Snihur,[34] A. Soha,[8] S. Somalwar,[52] V. Sorin,[36] J. Spalding,[18] T. Spreitzer,[34] P. Squillacioti,[46,g] M. Stanitzki,[60] R. St. Denis,[22] B. Stelzer,[9] O. Stelzer-Chilton,[42] D. Stentz,[38] J. Strologas,[37] D. Stuart,[11] J. S. Suh,[28] A. Sukhanov,[19] I. Suslov,[16] T. Suzuki,[55] A. Taffard,[25,s] R. Takashima,[40] Y. Takeuchi,[55] R. Tanaka,[40] M. Tecchio,[35] P. K. Teng,[1] K. Terashi,[50] J. Thom,[18,t] A. S. Thompson,[22] G. A. Thompson,[25] E. Thomson,[45] P. Tipton,[60] V. Tiwari,[13] S. Tkaczyk,[18] D. Toback,[53] S. Tokar,[15] K. Tollefson,[36] T. Tomura,[55] D. Tonelli,[18] S. Torre,[20] D. Torretta,[18] P. Totaro,[54,h] S. Tourneur,[44] Y. Tu,[45] N. Turini,[46,g] F. Ukegawa,[55] S. Vallecorsa,[21] N. van Remortel,[24,u] A. Varganov,[35] E. Vataga,[46,b] F. Vázquez,[19,e] G. Velev,[18] C. Vellidis,[3] V. Veszpremi,[48] M. Vidal,[32] R. Vidal,[18] I. Vila,[12] R. Vilar,[12] T. Vine,[31] M. Vogel,[37] I. Volobouev,[29,m] G. Volpi,[46,c] F. Würthwein,[10] P. Wagner,[2] R. G. Wagner,[2] R. L. Wagner,[18] J. Wagner-Kuhr,[27] W. Wagner,[27] T. Wakisaka,[41] R. Wallny,[9] S. M. Wang,[1] A. Warburton,[34] D. Waters,[31] M. Weinberger,[53] W. C. Wester III,[18] B. Whitehouse,[56] D. Whiteson,[45,s] A. B. Wicklund,[2] E. Wicklund,[18] G. Williams,[34] H. H. Williams,[45] P. Wilson,[18] B. L. Winer,[39] P. Wittich,[18,t] S. Wolbers,[18] C. Wolfe,[14] T. Wright,[35] X. Wu,[21] S. M. Wynne,[30] A. Yagil,[10] K. Yamamoto,[41] J. Yamaoka,[52] T. Yamashita,[40] U. K. Yang,[14,v] Y. C. Yang,[28] W. M. Yao,[29] G. P. Yeh,[18] J. Yoh,[18] K. Yorita,[14] T. Yoshida,[41] G. B. Yu,[49] I. Yu,[28] S. S. Yu,[18] J. C. Yun,[18] L. Zanello,[51,k] A. Zanetti,[54] I. Zaw,[23] X. Zhang,[25] Y. Zheng,[9,w] and S. Zucchelli[6,f]

(CDF Collaboration)

[1]*Institute of Physics, Academia Sinica, Taipei, Taiwan 11529, Republic of China*
[2]*Argonne National Laboratory, Argonne, Illinois 60439, USA*
[3]*University of Athens, 157 71 Athens, Greece*
[4]*Institut de Fisica d'Altes Energies, Universitat Autonoma de Barcelona, E-08193, Bellaterra (Barcelona), Spain*
[5]*Baylor University, Waco, Texas 76798, USA*
[6]*Istituto Nazionale di Fisica Nucleare Bologna, I-40127 Bologna, Italy*
[7]*Brandeis University, Waltham, Massachusetts 02254, USA*
[8]*University of California, Davis, Davis, California 95616, USA*
[9]*University of California, Los Angeles, Los Angeles, California 90024, USA*
[10]*University of California, San Diego, La Jolla, California 92093, USA*
[11]*University of California, Santa Barbara, Santa Barbara, California 93106, USA*
[12]*Instituto de Fisica de Cantabria, CSIC-University of Cantabria, 39005 Santander, Spain*
[13]*Carnegie Mellon University, Pittsburgh, Pennsylvania 15213, USA*
[14]*Enrico Fermi Institute, University of Chicago, Chicago, Illinois 60637, USA*
[15]*Comenius University, 842 48 Bratislava, Slovakia; Institute of Experimental Physics, 040 01 Kosice, Slovakia*
[16]*Joint Institute for Nuclear Research, RU-141980 Dubna, Russia*
[17]*Duke University, Durham, North Carolina 27708, USA*
[18]*Fermi National Accelerator Laboratory, Batavia, Illinois 60510, USA*
[19]*University of Florida, Gainesville, Florida 32611, USA*
[20]*Laboratori Nazionali di Frascati, Istituto Nazionale di Fisica Nucleare, I-00044 Frascati, Italy*
[21]*University of Geneva, CH-1211 Geneva 4, Switzerland*
[22]*Glasgow University, Glasgow G12 8QQ, United Kingdom*
[23]*Harvard University, Cambridge, Massachusetts 02138, USA*
[24]*Division of High Energy Physics, Department of Physics, University of Helsinki and Helsinki Institute of Physics, FIN-00014, Helsinki, Finland*
[25]*University of Illinois, Urbana, Illinois 61801, USA*
[26]*The Johns Hopkins University, Baltimore, Maryland 21218, USA*

[27]*Institut für Experimentelle Kernphysik, Universität Karlsruhe, 76128 Karlsruhe, Germany*
[28]*Center for High Energy Physics: Kyungpook National University, Daegu 702-701, Korea; Seoul National University, Seoul 151-742, Korea; Sungkyunkwan University, Suwon 440-746, Korea; Korea Institute of Science and Technology Information, Daejeon, 305-806, Korea; Chonnam National University, Gwangju, 500-757, Korea*
[29]*Ernest Orlando Lawrence Berkeley National Laboratory, Berkeley, California 94720, USA*
[30]*University of Liverpool, Liverpool L69 7ZE, United Kingdom*
[31]*University College London, London WC1E 6BT, United Kingdom*
[32]*Centro de Investigaciones Energeticas, Medioambientales y Tecnologicas, E-28040 Madrid, Spain*
[33]*Massachusetts Institute of Technology, Cambridge, Massachusetts 02139, USA*
[34]*Institute of Particle Physics: McGill University, Montréal, Canada H3A 2T8; and University of Toronto, Toronto, Canada M5S 1A7*
[35]*University of Michigan, Ann Arbor, Michigan 48109, USA*
[36]*Michigan State University, East Lansing, Michigan 48824, USA*
[37]*University of New Mexico, Albuquerque, New Mexico 87131, USA*
[38]*Northwestern University, Evanston, Illinois 60208, USA*
[39]*The Ohio State University, Columbus, Ohio 43210, USA*
[40]*Okayama University, Okayama 700-8530, Japan*
[41]*Osaka City University, Osaka 588, Japan*
[42]*University of Oxford, Oxford OX1 3RH, United Kingdom*
[43]*Istituto Nazionale di Fisica Nucleare, Sezione di Padova-Trento, I-35131 Padova, Italy*
[44]*LPNHE, Universite Pierre et Marie Curie/IN2P3-CNRS, UMR7585, Paris, F-75252 France*
[45]*University of Pennsylvania, Philadelphia, Pennsylvania 19104, USA*
[46]*Istituto Nazionale di Fisica Nucleare Pisa, I-56127 Pisa, Italy*
[47]*University of Pittsburgh, Pittsburgh, Pennsylvania 15260, USA*
[48]*Purdue University, West Lafayette, Indiana 47907, USA*
[49]*University of Rochester, Rochester, New York 14627, USA*
[50]*The Rockefeller University, New York, New York 10021, USA*
[51]*Istituto Nazionale di Fisica Nucleare, Sezione di Roma 1, I-00185 Roma, Italy*
[52]*Rutgers University, Piscataway, New Jersey 08855, USA*
[53]*Texas A&M University, College Station, Texas 77843, USA*
[54]*Istituto Nazionale di Fisica Nucleare Trieste/Udine, Italy*
[55]*University of Tsukuba, Tsukuba, Ibaraki 305, Japan*
[56]*Tufts University, Medford, Massachusetts 02155, USA*
[57]*Waseda University, Tokyo 169, Japan*
[58]*Wayne State University, Detroit, Michigan 48201, USA*
[59]*University of Wisconsin, Madison, Wisconsin 53706, USA*
[60]*Yale University, New Haven, Connecticut 06520, USA*
(Received 25 March 2008; published 15 August 2008)

[a]Also at University of Padova, I-35131 Padova, Italy.
[b]Also at Scuola Normale Superiore, I-56127 Pisa, Italy.
[c]Also at University of Pisa, I-56127 Pisa, Italy.
[d]Visitor from IFIC (CSIC-Universitat de Valencia), 46071 Valencia, Spain.
[e]Visitor from Universidad Iberoamericana, Mexico D.F., Mexico.
[f]Also at University of Bologna, I-40127 Bologna, Italy.
[g]Also at University of Siena, I-56127 Pisa, Italy.
[h]Also at University of Trieste/Udine, Italy.
[i]Visitor from Queen Mary, University of London, London, E1 4NS, England.
[j]Visitor from University de Oviedo, E-33007 Oviedo, Spain.
[k]Also at Sapienza Università di Roma, I-00185 Roma, Italy.
[l]Visitor from University of Bristol, Bristol BS8 1TL, United Kingdom.
[m]Visitor from Texas Tech University, Lubbock, TX 79409.
[n]Visitor from University of Edinburgh, Edinburgh EH9 3JZ, United Kingdom.
[o]Visitor from University College Dublin, Dublin 4, Ireland.
[p]Visitor from University of California Santa Cruz, Santa Cruz, CA 95064.
[q]Visitor from University of Cyprus, Nicosia CY-1678, Cyprus.
[r]Visitor from Nagasaki Institute of Applied Science, Nagasaki, Japan.
[s]Visitor from University of California Irvine, Irvine, CA 92697.
[t]Visitor from Cornell University, Ithaca, NY 14853.
[u]Visitor from Universiteit Antwerpen, B-2610 Antwerp, Belgium.

We present a search for standard model Higgs boson production in association with a $W$ boson in proton-antiproton collisions ($p\bar{p} \to W^{\pm}H \to \ell\nu b\bar{b}$) at a center of mass energy of 1.96 TeV. The search employs data collected with the CDF II detector which correspond to an integrated luminosity of approximately 1 fb$^{-1}$. We select events consistent with a signature of a single lepton ($e^{\pm}/\mu^{\pm}$), missing transverse energy, and two jets. Jets corresponding to bottom quarks are identified with a secondary vertex tagging method and a neural network filter technique. The observed number of events and the dijet mass distributions are consistent with the standard model background expectations, and we set 95% confidence level upper limits on the production cross section times branching ratio ranging from 3.9 to 1.3 pb for Higgs boson masses from 110 to 150 GeV/$c^2$, respectively.

DOI: 10.1103/PhysRevD.78.032008 PACS numbers: 13.85.Rm, 14.80.Bn

## I. INTRODUCTION

Standard electroweak theory predicts a single fundamental scalar particle, the Higgs boson, which arises as a result of spontaneous electroweak symmetry breaking [1]; however, the Higgs boson has not been directly observed experimentally. The current constraint on the Higgs boson mass, $m_H > 114.4$ GeV/$c^2$ at 95% confidence level (C.L.), comes from direct searches at LEP2 experiments [2]. Global fits to electroweak measurements exclude masses above 144 GeV/$c^2$ at 95% C.L. [3].

At the Tevatron $p\bar{p}$ collider at Fermilab, the next-to-leading-order (NLO) Higgs boson production cross section by gluon fusion is about ten times larger than for $WH$ associated production, and the cross section for $WH$ is about twice that of $ZH$ [4]. The Higgs boson decay branching ratio is dominated by $H \to b\bar{b}$ for $m_H < 135$ GeV/$c^2$ and by $H \to W^+W^-$ for $m_H > 135$ GeV/$c^2$ [5]. Background QCD $b\bar{b}$ production processes in the same invariant mass range have cross sections at least 4 orders of magnitude greater than that of Higgs boson production [6], and this renders searches in the $gg \to H \to b\bar{b}$ channel extremely difficult. However, requiring the leptonic decay of the associated weak boson reduces the huge QCD background rate. As a result, $WH \to \ell\nu b\bar{b}$ is considered to be one of the most sensitive processes for low mass Higgs boson searches.[1]

Searches for $WH \to \ell\nu b\bar{b}$ at $\sqrt{s} = 1.96$ TeV have been most recently reported by CDF (using data corresponding to an integrated luminosity of 319 pb$^{-1}$) [7] and D0 (440 pb$^{-1}$)[8]. The CDF analysis used a secondary vertex $b$-tagging algorithm (SECVTX) to distinguish $b$-quark jets from light-flavor or gluon jets [9]. Upper limits on the Higgs boson production rate, defined as the cross section times branching ratio ($\sigma \cdot \mathcal{B}$), were derived for mass hypotheses ranging from 110 to 150 GeV/$c^2$. The rate was constrained to be less than 10 pb at 95% C.L. for $m_H =$ 110 and less than 2.8 pb for 150 GeV/$c^2$. In that analysis, about 50% of the jets tagged by the SECVTX tagging algorithm were actually falsely $b$-tagged jets originating from light-flavor, gluon, or charm quarks. This effect is due to the finite resolution of track measurements and the long lifetime of $D$ mesons. Even though the fraction of mistagged events is small in the dominant $Wq\bar{q}$ process, the total number of mistagged events is significant, even when compared to true $Wb\bar{b}$ production. This is due completely to the size of the $Wq\bar{q}$ cross section, which is nearly 2 orders of magnitude larger than the $Wb\bar{b}$ cross section. To reduce this contamination and enhance the $b$-jet purity of our sample, we introduce a $b$-tagging neural network filter which uses as inputs jet characteristics as well as secondary vertex information.

In this paper, we present a search for $WH \to \ell\nu b\bar{b}$ production at CDF using about 1 fb$^{-1}$ of data. Section II describes the CDF II detector. The event selection criteria are explained in Sec. III. In Sec. IV, the $b$-tagging algorithm with SECVTX and neural network (NN) are discussed in detail. Contributions from the standard model (SM) background are calculated in Sec. V for various sources. In Sec. VI, signal acceptance and systematic uncertainties are estimated. The search optimization and statistical interpretation of the results are presented in Secs. VII and VIII, respectively. Finally, our conclusions are presented in Sec. IX.

## II. CDF II DETECTOR

The CDF II detector geometry is described using a cylindrical coordinate system [10]. The $z$ axis follows the proton direction, and the polar angle $\theta$ is usually expressed through the pseudorapidity $\eta = -\ln(\tan(\theta/2))$. The detector is approximately symmetric in $\eta$ and in the azimuthal angle $\phi$.

Charged particles are tracked by a system of silicon microstrip detectors and a large open cell drift chamber in the region $|\eta| \leq 2.0$ and $|\eta| \leq 1.0$, respectively. The tracking detectors are immersed in a 1.4 T solenoidal magnetic field aligned coaxially with the incoming beams, allowing measurement of charged particle momentum transverse to the beam line.

The resolution on the transverse momentum $p_T = p\sin\theta$ is measured to be $\delta p_T/p_T \approx 0.1\% \cdot p_T$ (GeV) for the combined tracking system. The resolution on the

[1]In this paper, lepton ($\ell$) denotes electron ($e^{\pm}$) or muon ($\mu^{\pm}$), and neutrino ($\nu$) denotes electron neutrino ($e_{\nu}$) or muon neutrino ($\mu_{\nu}$).

track impact parameter ($d_0$), or distance from the beam line axis to the track at the track's closest approach in the transverse plane, is $\sigma(d_0) \approx 40\ \mu$m, about 30 $\mu$m of which is due to the transverse size of the Tevatron interaction region.

Outside of the tracking systems and the solenoid, segmented calorimeters with projective tower geometry are used to reconstruct electromagnetic showers and hadronic jets [11–13] over the pseudorapidity range $|\eta| < 3.6$. A transverse energy $E_T = E\sin\theta$ is measured in each calorimeter tower where the polar angle ($\theta$) is calculated using the measured $z$ position of the event vertex and the tower location.

Small contiguous groups of calorimeter towers with signals are identified and summed together into an energy cluster. Electron candidates are identified in the central electromagnetic calorimeter (CEM) as isolated, mostly electromagnetic clusters which match a track in the pseudorapidity range $|\eta| < 1.1$. The electron transverse energy is reconstructed from the electromagnetic cluster with a resolution $\sigma(E_T)/E_T = 13.5\%/\sqrt{E_T/(\mathrm{GeV})} \oplus 2\%$ [11]. Jets are identified as a group of electromagnetic (EM) and hadronic (HAD) calorimeter clusters which fall within a cone of radius $\Delta R = \sqrt{\Delta\phi^2 + \Delta\eta^2} \leq 0.4$ units around a high-$E_T$ seed cluster [14]. Jet energies are corrected for calorimeter nonlinearity, losses in the gaps between towers, multiple primary interactions, out-of-cone losses, and inflow from the underlying event [15].

For this analysis, muons are detected in three separate subdetectors. After at least five interaction lengths in the calorimeter, the muons first encounter four layers of planar drift chambers (CMU), capable of detecting muons with $p_T > 1.4$ GeV/$c$ [16]. Four additional layers of planar drift chambers (CMP) behind another 60 cm of steel detect muons with $p_T > 2.8$ GeV/$c$ [17]. These two systems cover the same central pseudorapidity region with $|\eta| \leq 0.6$. Muons which exit the calorimeters at $0.6 \leq |\eta| \leq 1.0$ are tracked by the CMX detector, consisting of four layers of drift chambers. Muon candidates are then identified as isolated tracks which extrapolate to line segments or ''stubs'' in one of the muon subdetectors. A track which is linked to both CMU and CMP stubs is called a CMUP muon.

The CDF trigger system is a three-level filter, with tracking information available even at the first level [18]. Events used in this analysis have all passed the high-energy electron or muon trigger selection. The first stage of the central electron trigger requires a track with $p_T > 8$ GeV/$c$ pointing to a tower with $E_T > 8$ GeV and $E_{\mathrm{HAD}}/E_{\mathrm{EM}} < 0.125$. The first stage of the muon trigger requires a track with $p_T > 4$ GeV/$c$ (CMUP) or 8 GeV/$c$ (CMX) pointing to a muon stub. A complete lepton reconstruction is performed online in the final trigger stage, where we require $E_T > 18$ GeV/$c^2$ for electrons and $p_T > 18$ GeV/$c$ for muons.

## III. EVENT SELECTION

The observable final state from the $WH \to \ell\nu b\bar{b}$ signal consists of two jets plus a lepton and missing transverse energy. The leptonic $W$ decay requirement in $WH$ events yields the high-$p_T$ lepton and large missing transverse energy due to the neutrino.

The results presented here use data collected between February 2002 and February 2006. The data collected using the CEM and CMUP triggers correspond to $955 \pm 57$ pb$^{-1}$, while the data from the CMX trigger corresponds to $941 \pm 56$ pb$^{-1}$.

The missing transverse energy ($\not\!\!E_T$) is a reconstructed quantity that is defined as the opposite of the vector sum of all calorimeter tower energy depositions projected on the transverse plane. It is often used as a measure of the sum of the transverse momenta of the particles that escape detection, most notably neutrinos. To be more readily interpretable as such, the raw $\not\!\!E_T$ vector is adjusted for corrected jet energies, for the transverse momentum of the muons, and for the energy deposition of any minimum ionizing high-$p_T$ muons.

Events are considered as $WH$ candidates only if they have exactly one high-$p_T$ isolated lepton [19], with $E_T > 20$ GeV for electrons or $p_T > 20$ GeV/$c$ for muons. The isolation cone of $\Delta R = 0.4$ surrounding the lepton must have less than 10% of the lepton energy. A primary event vertex position is calculated by fitting a subset of particle tracks which are consistent with having come from the beam line. The distance between this primary event vertex and the lepton track $z_0$ must be less than 5 cm to ensure the lepton and the jets come from the same hard interaction. Some leptonic $Z$ decays would mimic the single-lepton signature if a lepton is unidentified. Events are therefore rejected if a second track with $p_T > 10$ GeV/$c$ forms an invariant mass with the lepton which falls in the $Z$-boson mass window ($76 < m_{\ell X} < 106$ GeV/$c^2$). The selected events are required to have $\not\!\!E_T$ greater than 20 GeV.

The $WH$ signal includes two jets originating from $H \to b\bar{b}$ decays; these jets are expected to have large transverse energy. The jets are required to be in the pseudorapidity range covered by the silicon detector so that secondary vertices from $b$ decays can be reconstructed. Specifically, we require the jets satisfy $E_T > 15$ GeV and $|\eta| < 2.0$. The search for $WH \to \ell\nu b\bar{b}$ is performed in the sample of events with $W$ + exactly 2 jets; however, samples of events with $W + 1$, 3, $\geq 4$ jets are used to cross-check the background modeling.

To increase the signal purity of the $W$ + 2-jet events, at least one jet must be $b$-tagged by the SECVTX algorithm. If only one of the jets is $b$-tagged, the jet must also pass the NN $b$-tagging filter. If there are two or more SECVTX $b$-tagged jets, the NN is not applied. With a SECVTX mistag rate of 1%, it is rare that two or more jets in the same events are mistagged by SECVTX.

## IV. SECONDARY VERTEX *b*-TAGGING

Multijet final states have dominant contributions from QCD light-flavor jet production, but the standard model Higgs boson decays predominantly to bottom quark pairs. Correctly identifying the $b$ quark jets helps to remove most of the QCD background. An algorithm has been developed and used to tag displaced secondary vertices from $b$ quark decays; however, the sample tagged by the SECVTX algorithm still has significant contamination from falsely tagged light-flavor or gluon jets and the misidentification of $c$ quarks as $b$-jets [20]. This search introduces a multivariate NN technique intended to improve the SECVTX tagging purity.

The $b$-quark has a relatively long lifetime, and $B$ hadrons formed during the hadronization of the initial $b$ quark can travel a significant distance on the order of millimeters before decaying into a collection of lighter hadrons. The decay vertex can be reconstructed by identifying tracks which form a secondary vertex significantly displaced from the $p\bar{p}$ interaction point (primary vertex).

The SECVTX $b$-tagging algorithm is applied to each jet in the event, using only the tracks which are within $\eta$-$\phi$ distance of $\Delta R = 0.4$ of the jet direction. Displaced tracks in jets are used for the SECVTX reconstruction and are distinguished by a large impact parameter significance ($|d_0/\sigma_{d_0}|$) where $d_0$ and $\sigma_{d_0}$ are the impact parameter and the total uncertainty from tracking and beam position measurements. Secondary vertices are reconstructed with a two-pass approach which tests for high-quality vertices in the first pass and allows lower-quality vertices in the second pass. In pass 1, at least three tracks are required to pass loose selection criteria ($p_T > 0.5$ GeV/$c$, $|d_0/\sigma_{d_0}| > 2.0$), and a secondary vertex is fit from the selected tracks. One of the tracks used in the reconstruction is required to have $p_T > 1.0$ GeV/$c$. If pass 1 fails, then a vertex is sought in pass 2 from at least two tracks satisfying tight selection criteria ($p_T > 1.0$ GeV/$c$, $|d_0/\sigma_{d_0}| > 3.5$ and one of the pass 2 tracks must have $p_T > 1.5$ GeV/$c$). If either pass is successful, the transverse distance ($L_{xy}$) from the primary vertex of the event is calculated along with the associated uncertainty. This uncertainty $\sigma_{L_{xy}}$ includes the uncertainty on the primary vertex position. Finally, jets are tagged positively or negatively depending on the $L_{xy}$ significance ($L_{xy}/\sigma_{L_{xy}}$):

$$L_{xy}/\sigma_{L_{xy}} \geq 7.5 \qquad \text{(positive tag)} \tag{1}$$

$$L_{xy}/\sigma_{L_{xy}} \leq -7.5 \qquad \text{(negative tag).} \tag{2}$$

These values have been tuned for optimum efficiency and purity in simulated $b$-jet samples from decays of top quarks. The energy spectrum for those jets is similar to the spectrum for $b$ jets from decays of Higgs bosons.

The sign of $L_{xy}$ indicates the position of the secondary vertex with respect to the primary vertex along the direction of the jet. If the angle between the jet axis and the vector pointing from the primary vertex to the secondary vertex is less than $\pi/2$, $L_{xy}$ is positively defined; otherwise, it is negative. If $L_{xy}$ is positive, the secondary vertex points towards the direction of the jet, as in true $B$ hadron decays. For negative $L_{xy}$ the secondary vertex points away from the jet; this may happen as a result of mismeasured tracks, so jets tagged with a negative $L_{xy}$ are labeled mistagged jets. In order to reject secondary vertices due to material interaction, the algorithm vetoes two-track vertices found between 1.2 and 1.5 cm from the center of the silicon detector (the inner radius of the beampipe and the outer radius of the innermost silicon layer being within this range). All vertices more than 2.5 cm from the center are rejected.

The negative tags are useful for evaluating the rate of false positive tags, which are defined "mistags" in the background estimates. Mismeasurements are expected to occur randomly; therefore the $L_{xy}$ distribution of fake tags is expected to be symmetric with respect to zero. Simulated events are used to correct a small asymmetry due to true long-lived particles in light-flavor jets.

The efficiency for identifying a secondary vertex is found to be different in the simulated and observed data sets. We measure an efficiency scale factor, which is defined as the ratio of the observed to the simulated efficiencies, to be $0.91 \pm 0.06$ in a sample of high-$E_T$ jets enriched in $b$ jets by requiring a soft lepton ($p_T > 8$ GeV/$c^2$) from semileptonic heavy quark decays [9].

Secondary vertex SECVTX $b$-tagging exploits the long lifetime of $B$ hadrons. $D$ hadrons originating from $c$-quarks also have fairly long lifetime, and secondary vertices in $c$-jets are frequently tagged. Therefore jets tagged by SECVTX are contaminated not only by falsely tagged light-flavor ($uds$ or gluon) jets, but also by long-lived charmed hadrons in $c$-jets. A neural network has been developed to filter the $b$-tagging results in order to improve the $b$-tagging purity.

The neural network used in this article employs the JETNET [21] package. The tagger is designed with two networks in series. The $b - l$ network is trained to separate $b$-jets from light-quark jets ($l$-jets), and the $b - c$ network is trained to separate $b$-jets from $c$-jets. Jets which pass a cut on both of the NN outputs are accepted by the tagger. These neural networks are trained and applied only to events which are already tagged by the SECVTX algorithm. The current NN $b$-tagging is tuned to increase the purity of the SECVTX $b$-tagged jets, not to increase the tagging efficiency.

The neural networks take as input the 16 variables listed in Table I. These variables are chosen primarily because the $b$-quark jets have higher track multiplicity, larger invariant mass, longer lifetime, and a harder fragmentation function than $c$- and $l$-quark jets. The track parameters and $L_{xy}$ significance are good discriminators for $b$-jets. The

TABLE I. Input variables used in the NN $b$-tagging filter. The variables in the first column are properties of the identified secondary vertex, while variables in the second column are jet properties independent of any identified vertex.

| SECVTX variable | SECVTX-independent variable |
|---|---|
| Number of tracks in fitted vertex | Number of good tracks |
| Vertex fit $\chi^2$ | Jet probability [22] |
| Transverse decay length ($L_{xy}$) | Reconstructed mass of pass 1 tracks |
| $L_{xy}$ significance ($L_{xy}/\sigma_{L_{xy}}$) | Reconstructed mass of pass 2 tracks |
| Vertex mass ($M_{\rm vtx} = \sqrt{(\sum \lvert \boldsymbol{p}_{\rm vtx}\rvert)^2 - (\sum \boldsymbol{p}_{\rm vtx})^2}$) | Number of pass 1 tracks |
| Pseudo-$c\tau$ ($L_{xy} \times M_{\rm vtx}/p_T^{\rm vtx}$) | Number of pass 2 tracks |
| $p_T^{\rm vtx}/(\sum_{\rm good\ tracks} p_T)$ | $\sum_{\rm Pass1\ track} p_T/p_T^{\rm jet}$ |
| Vertex pass number (pass 1 or 2) | $\sum_{\rm Pass2\ track} p_T/p_T^{\rm jet}$ |

vertex $p_T^{\rm VTX}$ and invariant mass $M_{\rm VTX}$ are useful variables for identifying $l$-jets; however $c$-jets have $p_T$ spectra similar to $b$-jets. Pseudo-$c\tau$ ($L_{xy} \times M_{\rm VTX}/p_T^{\rm VTX}$), the vertex fit $\chi^2$, and the track-based probability of a jet to come from the primary vertex are the best discriminators. The outputs of the two neural networks are shown in Fig. 1.

The NN $b$-tagger is validated by comparing the performance on data and Monte Carlo dijet events in a special calibration sample. In this sample, triggered by an electron candidate with $E_T > 8$ GeV, events are selected in which two jets are tagged by the SECVTX algorithm. The sample composition is nearly pure $b\bar{b}$, where one $b$ jet includes a semileptonic decay. The NN outputs from the $b - l$ network are shown in Fig. 2 for a sample of SECVTX tagged heavy-flavor jets from such events in data and in the corresponding $b\bar{b}$ Monte Carlo sample. The outputs of the $b - l$ network on tagged light-flavor jets are also shown for data and Monte Carlo. Figure 2 shows the good agreement in NN $b$-tagger performance between data and Monte Carlo.

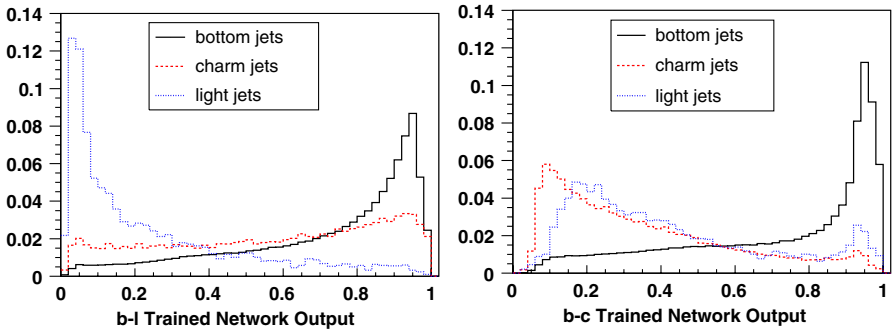


FIG. 1 (color online). Neural network outputs obtained from trainings of $b$ vs $l$ jets (left) and $b$ vs $c$ jets (right). Output distributions for $b$, $c$, and $l$ jets are shown in solid, dashed, and dotted lines, respectively.

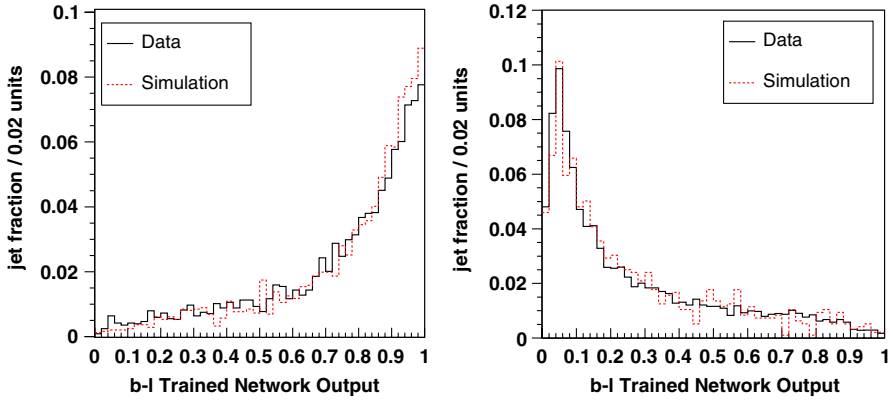


FIG. 2 (color online). Comparisons of NN $b$-tag output in data (solid line), and Monte Carlo (dashed line) for SECVTX-tagged heavy-flavor-enriched jets (left) and tagged light-flavor jets (right).

We tune the cut values for 90% $b$ efficiency (after the SECVTX efficiency), corresponding to values of $\mathrm{NN}_{b-l} = 0.182$ and $\mathrm{NN}_{b-c} = 0.242$. The data-to-Monte-Carlo scale factor, measured from the electron sample, is $0.97 \pm 0.02$. Note that this is an additional scale factor with respect to the SECVTX efficiency scale factor because all of the jets under consideration have already been tagged by SECVTX. At these cut values, the NN filter rejects 65% of light-flavor jets and about 50% of the $c$ jets while keeping 90% of $b$-jets after being tagged by SECVTX.

## V. BACKGROUND

The final state signature from $WH \rightarrow \ell\nu b\bar{b}$ production can also be reached by other production processes. The main background processes are $W$ + jets production, $t\bar{t}$ production, and non-$W$ QCD multijet production. Several electroweak production processes also contribute with smaller background rates. In the following subsections the contribution from each background source is calculated in detail.

### A. Non-$W$ QCD multijet

Events from QCD multijet production sometimes mimic the $W$-boson signature with fake leptons or fake $\not\!\!E_T$. Non-$W$ leptons are reconstructed when a jet passes the lepton selection criteria or a heavy-flavor jet produces leptons via semileptonic decay. Non-$W$ $\not\!\!E_T$ can be observed via mismeasurements of energy or semileptonic decays of heavy-flavor quarks. It is difficult to model and produce the former class of events in detector simulation since the reasons for mismeasurement are not known quantitatively. Instead, we estimate the contribution of non-$W$ events directly from the data sample before $b$-tagging is applied.

Generally, the bulk of non-$W$ events are characterized by a nonisolated lepton and small $\not\!\!E_T$. Lepton isolation $I$ is defined as the ratio of calorimeter energy inside a cone of $\Delta R = 0.4$ about the lepton to the lepton energy itself. The quantity $I$ is small if the lepton is well-isolated from the rest of the event, as typified by a true leptonic $W$ decay. This feature is used to extrapolate the expected non-$W$ contribution into our signal region, namely, small $I$ and large $\not\!\!E_T$. The following 4 sideband sectors are used for the extrapolation: $I > 0.2$ and $\not\!\!E_T < 15$ GeV (region $A$), $I < 0.1$ and $\not\!\!E_T < 15$ GeV (region $B$), $I > 0.2$ and $\not\!\!E_T > 20$ GeV (region $C$), and $I < 0.1$ and $\not\!\!E_T > 20$ GeV (region $D$). Here, region $D$ corresponds to the signal region. In extracting the non-$W$ background contribution from data, we make the following two assumptions: lepton isolation and $\not\!\!E_T$ are uncorrelated in non-$W$ events, and the $b$-tagging rate is not dependent on $\not\!\!E_T$ in non-$W$ events. The level at which these assumptions are justified determines the assigned uncertainty.

With the first assumption, the number of non-$W$ events ($N_D^{\text{non-}W}$) and their relative fraction in the signal region before requiring $b$-tagging ($f_{\text{non-}W}$) obey the following relations:

$$N_D^{\text{non-}W} = \frac{N_B \times N_C}{N_A}, \tag{3}$$

$$f_{\text{non-}W} = \frac{N_D^{\text{non-}W}}{N_D} = \frac{N_B \times N_C}{N_A \times N_D}, \tag{4}$$

where $N_i (i = A, B, C, D)$ are the number of pretag events in each sideband region. The number of pretag events has been corrected for known sources of prompt leptons. By invoking the second assumption, the SECVTX $b$-tagging efficiency obtained in region $B$ can be applied to the signal region $D$. Here we define an event tagging efficiency per taggable jet (one with at least two good SECVTX tracks) as follows:

$$r_B = \frac{N_B^{(\text{tagged event})}}{N_B^{(\text{taggable jet})}}, \tag{5}$$

where $N_B^{(\text{tagged event})}$ and $N_B^{(\text{taggable jet})}$ are the number of tagged events and taggable jets in region $B$, respectively. Then the number of non-$W$ background in region $D$ after SECVTX $b$-tagging ($N_D^{+\text{non-}W}$) is obtained by using the "tag rate" relation:

$$N_D^{+\text{non-}W} = f_{\text{non-}W} \times r_B \times N_D^{(\text{taggable jets})}. \tag{6}$$

It is also possible to estimate non-$W$ contribution solely from the SECVTX-tagged sample as

$$N_D^{\prime+\text{non-}W} = \frac{N_B^+ \times N_C^+}{N_A^+}, \tag{7}$$

where $N_X^+ (X = A, B, C, D)$ in the "tagged method" are the number of events with positive tags. These methods are data-based techniques, so the estimates could also contain other background processes. The contributions from $t\bar{t}$ and $W$ + jets events to each sideband region are subtracted according to the calculated cross sections for those processes, including the appropriate tagging efficiencies.

To validate the four-sector method and estimate their systematic uncertainties, we vary the boundaries of the four regions and divide the $I$ and $\not\!\!E_T$ sidebands into two sidebands: $E(0.1 < I < 0.2 \quad \text{and} \quad \not\!\!E_T > 20$ GeV) and $F(I < 0.1 \quad \text{and} \quad 15 < \not\!\!E_T < 20$ GeV). The observed deviations imply a 25% systematic uncertainty in the non-$W$ background yield, assigned conservatively for both the pretag and tagged estimates.

The independent estimates from the tag rate method [Eq. (6)] and the tagged method [Eq. (7)] are combined using a weighted average. The result from the tagged method gives a slightly higher estimate than the tag rate method, but the two results are consistent within the 25% uncertainty.

A non-$W$ rejection factor associated with the NN $b$-tagging filter is measured from data in region $C$. Region $C$ has event kinematics similar to non-$W$ events

in the signal region $D$ because lepton isolation is the only difference between the two regions. The non-$W$ estimate calculated before applying NN $b$-tagging is scaled by this NN rejection factor; this assumes the NN filter is uncorrelated with the isolation.

The non-$W$ estimate for events with at least two SECVTX tags is obtained by measuring the ratio of the number of events with at least one $b$-tag to the number with at least two $b$-tags in sideband regions and applying the ratio to the estimate of tagged non-$W$ events in the signal region $D$.

### B. Mistagged Jets

The rate at which SECVTX falsely tags light-flavor jets is derived from generic jet samples in varying bins of $\eta$, $\phi$, jet $E_T$, track multiplicity, and total event $E_T$ scalar sum. Tag rate probabilities are summed for all of the taggable jets in the event, jets with at least two tracks well measured in the silicon detector. Since the double-mistag rate is small, this sum is a good approximation of the single-tag event rate. Negative mistags—tags with unphysical negative decay length due to finite tracking resolution—are assumed to be a good estimate of falsely tagged jets, independent to first order of heavy-flavor content in the generic jet sample. The systematic uncertainty on the rate is largely due to self-consistency in the parametrization as applied to the generic jet sample. The positive mistag rate is enhanced relative to the negative tag rate by light-flavor secondary vertices and material interactions in the silicon detectors. As a result, the positive mistag rate is corrected by multiplying the negative mistag rate by a factor of $1.37 \pm 0.15$. This factor is measured in a control sample by fitting the asymmetry in the vertex mass distribution of positive tags over negative tags [23]. An additional correction factor of $1.05 \pm 0.03$ is applied for data collected after December 2004, when the Tevatron beam position changed slightly. The mistag rate per jet is applied to events in the $W$ + jets sample. The total estimate is corrected for the non-$W$ QCD fraction and also the top-quark contributions to the pretag sample. To estimate the mistag contribution in NN-tagged events, we apply the light-flavor rejection power of the NN filter $0.35 \pm 0.05$ as measured using light-flavor jets from various data and simulated samples.

### C. $W$ + heavy flavor

The $Wb\bar{b}$, $Wc\bar{c}$, and $Wc$ states are major background sources of secondary vertex tags. Large theoretical uncertainties exist for the overall normalization in part because current Monte Carlo programs generate $W$ + heavy-flavor events only to leading order. Consequently, rates for these processes are normalized to data. The contribution from true heavy-flavor production in $W$ + jets events is determined from measurements of the heavy-flavor event fraction in $W$ + jets events and the $b$-tagging efficiency for those events, as explained below.

TABLE II. The heavy-flavor fractions, given in percent, for the $W$ + jets sample. Quoted jet multiplicities are exclusive. The results from ALPGEN Monte Carlo have been scaled by the data-derived calibration factor of $1.5 \pm 0.4$. ($Wc$ fractions have not been rescaled.)

| Jet multiplicity | 1 jet | 2 jets | 3 jets | $\geq 4$ jets |
|---|---|---|---|---|
| $Wb\bar{b}$ (1B) (%) | $1.0 \pm 0.3$ | $1.4 \pm 0.4$ | $2.0 \pm 0.5$ | $2.2 \pm 0.6$ |
| $Wb\bar{b}$ (2B) (%) | ... | $1.4 \pm 0.4$ | $2.0 \pm 0.5$ | $2.6 \pm 0.7$ |
| $Wc\bar{c}$ (1C) (%) | $1.6 \pm 0.4$ | $2.4 \pm 0.6$ | $3.4 \pm 0.9$ | $3.6 \pm 1.0$ |
| $Wc\bar{c}$ (2C) (%) | ... | $1.8 \pm 0.5$ | $2.7 \pm 0.7$ | $3.7 \pm 1.0$ |
| $Wc$ (%) | $4.3 \pm 0.9$ | $6.0 \pm 1.3$ | $6.3 \pm 1.3$ | $6.1 \pm 1.3$ |

The fraction of $W$ + jets events produced with heavy-flavor jets has been studied extensively using an ALPGEN + HERWIG combination of Monte Carlo programs [24,25]. Calculations of the heavy-flavor fraction in ALPGEN have been calibrated using a jet data sample, and measurements indicate a scaling factor of $1.5 \pm 0.4$ is necessary to make the heavy-flavor production in Monte Carlo match the production in multijet data [9]. The final results of heavy-flavor fractions are obtained as shown in Table II. In the table, 1B and 1C refer to the case in which only one of the heavy-flavor jets is detected; this happens when one jet goes out of the detector coverage or when two parton jets merge into the same reconstructed jet. Similarly, 2B and 2C refer to the case in which both of the heavy-flavor jets are observed.

For the tagged $W$ + heavy flavor background estimate, the heavy-flavor fractions and tagging rates given in Tables II and III are multiplied by the number of pretag

TABLE III. The $b$-tagging efficiencies in percent for various $b$-tagging strategies on individual $W$ + heavy-flavor processes. Categories 1B, 2B refer to number of taggable $b$-jets in the events, with similar categories for charm jets. Those numbers include the effect of the data-to-Monte Carlo scale factors algorithm and the neural network filter.

| Jet Multiplicity | 1 jet | 2 jets | 3 jets | $\geq 4$ jets |
|---|---|---|---|---|
| $\geq 1$ SECVTX $b$-tag (%) | | | | |
| $Wb\bar{b}$ (1B) | $33.2 \pm 2.4$ | $34.5 \pm 2.5$ | $36.7 \pm 2.6$ | $40.2 \pm 2.9$ |
| $Wb\bar{b}$ (2B) | ... | $51.3 \pm 3.6$ | $54.1 \pm 3.8$ | $55.1 \pm 3.9$ |
| $Wc\bar{c}$ (1C) | $6.2 \pm 0.9$ | $8.0 \pm 1.1$ | $9.7 \pm 1.4$ | $11.6 \pm 1.6$ |
| $Wc\bar{c}$ (2C) | ... | $14.4 \pm 2.0$ | $17.0 \pm 2.4$ | $17.8 \pm 2.5$ |
| $Wc$ | $8.9 \pm 1.3$ | $8.7 \pm 1.2$ | $7.6 \pm 1.1$ | $3.4 \pm 0.5$ |
| $\geq 1$ SECVTX and NN $b$-tag (%) | | | | |
| $Wb\bar{b}$ (1B) | $29.9 \pm 2.1$ | $31.8 \pm 2.3$ | $34.1 \pm 2.4$ | $35.9 \pm 2.6$ |
| $Wb\bar{b}$ (2B) | ... | $47.2 \pm 3.4$ | $51.5 \pm 3.7$ | $51.3 \pm 3.6$ |
| $Wc\bar{c}$ (1C) | $3.8 \pm 0.5$ | $5.5 \pm 0.8$ | $6.1 \pm 0.9$ | $6.4 \pm 0.9$ |
| $Wc\bar{c}$ (2C) | ... | $9.9 \pm 1.4$ | $8.6 \pm 1.2$ | $9.5 \pm 1.4$ |
| $Wc$ | $5.0 \pm 0.7$ | $4.6 \pm 0.7$ | $3.1 \pm 0.4$ | $3.4 \pm 0.5$ |
| $\geq 2$ SECVTX $b$-tag (%) | | | | |
| $Wb\bar{b}$ (2B) | ... | $9.7 \pm 0.7$ | $13.6 \pm 1.0$ | $11.5 \pm 0.8$ |
| $Wc\bar{c}$ (2C) | ... | $1.2 \pm 0.2$ | $0.8 \pm 0.1$ | $0.9 \pm 0.1$ |

TABLE IV. Theoretical cross sections and uncertainties for the electroweak and single top backgrounds, along with the theoretical cross section for $t\bar{t}$ at $m_t = 175\ \mathrm{GeV}/c^2$. The cross section of $Z^0 \to \tau^+\tau^-$ is obtained in the dilepton mass range $m_{\tau\tau} > 30\ \mathrm{GeV}/c^2$ together with a $k$-factor (NLO/LO) of 1.4.

| Theoretical cross sections | |
|---|---|
| $WW$ | $12.40 \pm 0.80$ pb |
| $WZ$ | $3.96 \pm 0.06$ pb |
| $ZZ$ | $1.58 \pm 0.02$ pb |
| Single top $s$-channel | $0.88 \pm 0.05$ pb |
| Single top $t$-channel | $1.98 \pm 0.08$ pb |
| $Z \to \tau^+\tau^-$ | $320 \pm 9$ pb |
| $t\bar{t}$ | $6.7 + 0.7 - 0.9$ pb |

$W$ + jets candidate events in data, after correction for the contribution of non-$W$ and $t\bar{t}$ events to the pretag sample.

The previous CDF analysis using 319 $\mathrm{pb}^{-1}$ of data provided some evidence that the disagreement between the predicted and observed numbers of $W + 1$ jet and $W + 2$ jet events is due to the heavy-flavor fraction [7]. In this analysis, an updated correction factor of $1.2 \pm 0.2$, obtained by fitting tagged $W + 1$ jet events only, is applied to the heavy-flavor fraction. The $W$ + heavy flavor heavy-flavor background contribution is obtained by the following relation:

$$N_{W+\mathrm{HF}} = f_{\mathrm{HF}} \cdot \epsilon_{\mathrm{tag}} \cdot [N_{\mathrm{pretag}} \cdot (1 - f_{\text{non-}W}) - N_{\mathrm{TOP}} - N_{\mathrm{EWK}}], \quad (8)$$

where $f_{\mathrm{HF}}$ is the heavy-flavor fraction, $\epsilon_{\mathrm{tag}}$ is the tagging efficiency, $N_{\mathrm{TOP}}$ is the expected number of $t\bar{t}$ and single top events, and $N_{\mathrm{EWK}}$ is the expected number of $WW$, $WZ$, and $Z$ boson events.

### D. Top and electroweak backgrounds

Production of both single top-quark and top-quark pairs contributes to the tagged lepton + jets sample. Several electroweak boson production processes also contribute. $WW$ pairs can decay to a lepton, neutrino as missing energy, and two jets, one of which may be charm. $WZ$ events can decay to the signal $Wb\bar{b}$ or $Wc\bar{c}$ final state. Finally, $Z \to \tau^+\tau^-$ events can have one leptonic $\tau$ decay and one hadronic decay. The leptonic $\tau$ decay gives rise to a lepton + missing transverse energy, while the hadronic decay yields a narrow jet of hadrons with a nonzero lifetime.

The normalization of the diboson and single top backgrounds are based on the theoretical cross sections listed in Table IV, the luminosity, and the acceptance and $b$-tagging efficiency derived from Monte Carlo events [19,26–28]. The acceptance is corrected for lepton identification, trigger efficiencies, and the $z$ vertex cut. The tagging efficiency is always corrected by the $b$-tagging scale factor.

TABLE VI. Background estimate for events with at least two SECVTX $b$-tagged jets as a function of exclusive jet multiplicity.

| Jet multiplicity | 2 jets | 3 jets | $\geq 4$ jets |
|---|---|---|---|
| Pretag events | 14604 | 2362 | 646 |
| Mistag | $3.5 \pm 0.5$ | $2.0 \pm 0.3$ | $1.2 \pm 0.2$ |
| $Wb\bar{b}$ | $20.3 \pm 7.0$ | $5.7 \pm 1.8$ | $1.0 \pm 0.4$ |
| $Wc\bar{c}$ | $3.3 \pm 1.1$ | $0.4 \pm 0.1$ | $0.1 \pm 0.04$ |
| $Wc$ | ... | ... | ... |
| $t\bar{t}$ (6.7 pb) | $10.4 \pm 2.3$ | $29.5 \pm 6.4$ | $45.5 \pm 9.9$ |
| Single top | $4.2 \pm 0.7$ | $1.4 \pm 0.2$ | $0.3 \pm 0.1$ |
| Diboson/$Z^0 \to \tau^+\tau^-$ | $1.2 \pm 0.3$ | $0.3 \pm 0.1$ | $0.1 \pm 0.1$ |
| Non-$W$ QCD | $1.4 \pm 0.3$ | $0.9 \pm 0.2$ | $0.3 \pm 0.1$ |
| Total background | $44.2 \pm 8.5$ | $40.1 \pm 6.8$ | $48.6 \pm 10.0$ |
| Observed events | 39 | 44 | 65 |

### E. Summary of background estimate

We have described the contributions of individual background sources to the final background estimate. The background estimates for the condition of exactly one $b$-tagged jet after applying the NN filter and at least two SECVTX $b$-tagged jets are summarized in Tables V and VI. The estimates are plotted in Figs. 3 and 4 for the case of

TABLE V. Background estimate for events with exactly one SECVTX $b$-tag that passes the NN filter as a function of exclusive jet multiplicity.

| Jet multiplicity | 1 jet | 2 jets | 3 jets | $\geq 4$ jets |
|---|---|---|---|---|
| Pretag events | 94051 | 14604 | 2362 | 646 |
| Mistag | $139.7 \pm 27.3$ | $53.9 \pm 10.7$ | $15.7 \pm 3.1$ | $4.2 \pm 0.8$ |
| $Wb\bar{b}$ | $306.9 \pm 106.9$ | $144.7 \pm 49.4$ | $29.9 \pm 9.7$ | $6.4 \pm 2.5$ |
| $Wc\bar{c}$ | $63.1 \pm 22.0$ | $43.0 \pm 14.7$ | $8.7 \pm 2.8$ | $1.9 \pm 0.8$ |
| $Wc$ | $185.7 \pm 47.2$ | $34.4 \pm 9.0$ | $3.4 \pm 0.9$ | $0.6 \pm 0.2$ |
| $t\bar{t}$(6.7 pb) | $6.9 \pm 1.2$ | $42.0 \pm 6.6$ | $84.9 \pm 12.8$ | $98.6 \pm 14.3$ |
| Single top | $16.7 \pm 1.8$ | $23.5 \pm 2.4$ | $4.8 \pm 0.5$ | $0.8 \pm 0.1$ |
| Diboson/$Z^0 \to \tau^+\tau^-$ | $11.7 \pm 2.2$ | $14.2 \pm 2.3$ | $3.9 \pm 0.9$ | $1.0 \pm 0.3$ |
| Non-$W$ QCD | $84.2 \pm 14.1$ | $38.9 \pm 6.7$ | $12.1 \pm 2.3$ | $5.5 \pm 1.2$ |
| Total background | $814.9 \pm 140.7$ | $394.4 \pm 66.6$ | $163.4 \pm 18.7$ | $118.9 \pm 14.9$ |
| Observed events | 856 | 421 | 177 | 139 |

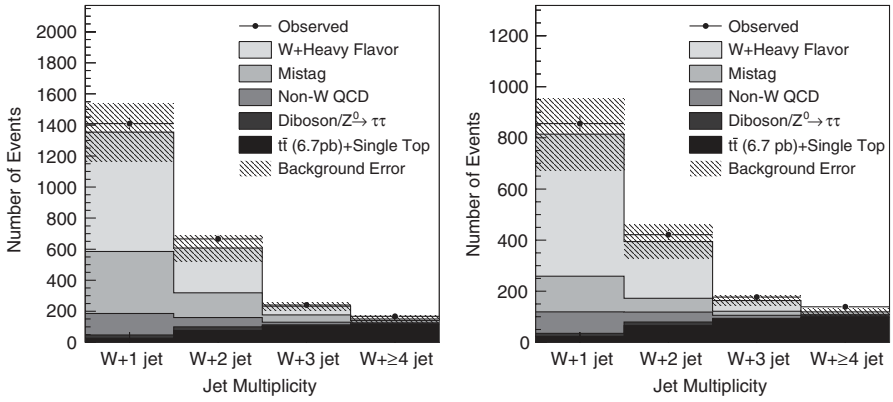


FIG. 3. Number of events as a function of exclusive jet multiplicity for events with exactly one SECVTX $b$-tag before (left) and after (right) applying the NN $b$-tagging requirement.

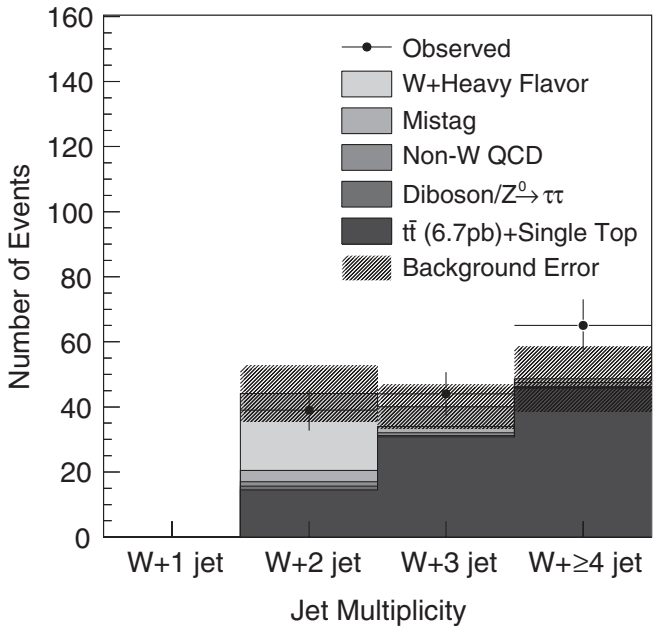


FIG. 4. Number of events as a function of exclusive jet multiplicity for events with at least two SECVTX $b$-tagged jets.

exactly one $b$-tag before and after applying the NN $b$-tag filter. The observed number of events in the data and the SM background expectations are consistent both before and after NN $b$-tagging is applied. The same is true for the number of events with at least two $b$-tagged jets. (See Table VI and Fig. 4.)

## VI. HIGGS BOSON SIGNAL ACCEPTANCE

The kinematics of the SM $WH \to \ell\nu b\bar{b}$ process are well defined, and events can be simulated accurately by Monte Carlo programs. The PYTHIA program was used to generate the signal samples [29]. Only Higgs boson masses between 110 and 150 GeV/$c^2$ are considered because this is the mass region for which the decay $H \to b\bar{b}$ dominates. The number of expected $WH \to \ell\nu b\bar{b}$ events $N$ is given by

$$N = \epsilon \cdot \int \mathcal{L}dt \cdot \sigma(p\bar{p} \to WH) \cdot \mathcal{B}(H \to b\bar{b}), \quad (9)$$

where $\epsilon$, $\int \mathcal{L}dt$, $\sigma(p\bar{p} \to WH)$, and $\mathcal{B}(H \to b\bar{b})$ are the event detection efficiency, integrated luminosity, production cross section, and branching ratio, respectively. The production cross section and branching ratio are calculated to NLO precision [5]. The acceptance $\epsilon$ is broken down into the following factors:

$$\epsilon = \sum_{\ell=e,\mu,\tau} (\epsilon_{z_0} \cdot \epsilon_{\text{trigger}} \cdot \epsilon_{\text{lepton ID}} \cdot \epsilon_{b\text{tag}} \cdot \epsilon_{\text{kinematics}} \cdot \mathcal{B}(W \to \ell\nu)), \quad (10)$$

where $\epsilon_{z_0}$, $\epsilon_{\text{trigger}}$, $\epsilon_{\text{lepton ID}}$, $\epsilon_{b\text{tag}}$, and $\epsilon_{\text{kinematics}}$ are efficiencies to meet the requirements of primary vertex, trigger, lepton identification, $b$-tagging, and kinematics. The major sources of inefficiency are the lepton identification, jet kinematics, and $b$-tagging factors; each is a factor between 0.3 and 0.45. The factor $\epsilon_{z_0}$ is obtained from data, and the others are calculated using Monte Carlo samples. The total signal acceptances for various $b$-tagging options including all systematic uncertainties as a function of Higgs boson mass are shown in Fig. 5.

The expected number of signal events is estimated by Eq. (9) at each Higgs boson mass point. The expectations for various $b$-tagging strategies are shown in Table VII. The NN $b$-tagging filter keeps about 90% of signal while it removes 35% of the total background in $W + 2$ jet events as shown in Fig. 3.

The total systematic uncertainty on the acceptance stems from the jet energy scale, initial and final state radiation, lepton identification, trigger efficiencies, and $b$-tagging. A 2% uncertainty on the lepton identification efficiency is assigned for each lepton type (CEM electron, CMUP and CMX muon), based on studies of $Z$ boson events. For each of the high $p_T$ lepton triggers, a 1% uncertainty is measured from backup trigger paths or $Z$ boson events. The

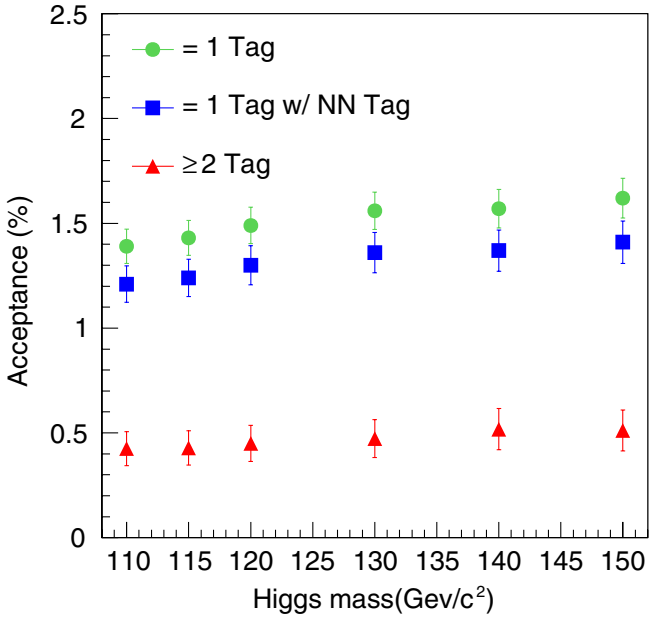


FIG. 5 (color online). The summary of acceptance of the process $WH \to \ell\nu b\bar{b}$ in $W + 2$ jet bin for various $b$-tagging strategies as a function of Higgs boson mass.

systematic uncertainties due to initial state radiation (ISR) and final state radiation (FSR) are estimated by changing the parameters related to ISR and FSR from their nominal values to half or double the nominal [30]. The difference from the nominal acceptance is taken as the systematic uncertainty. The uncertainty in the incoming parton energies relies on the eigenvalue uncertainties provided in the PDF fits. An NLO version of the PDFs, CTEQ6M, provides variations in the fits corresponding to 100 units in $\chi^2$ for each of 20 eigenvectors [31]. The nominal PDF value is reweighted to the value from each uncertainty set in turn, and the corresponding reweighted acceptance is computed. The differences between nominal and reweighted acceptances are added in quadrature, and the total is assigned as the systematic uncertainty [9].

The uncertainty due to the jet energy scale uncertainty (JES) [15] is calculated by shifting jet energies in $WH$ Monte Carlo samples by $\pm 1\sigma$. The deviation from the nominal acceptance is taken as the systematic uncertainty.

TABLE VII. Expected number of $WH \to \ell\nu b\bar{b}$ signal events with systematic uncertainties for various $b$-tagging options, where "tag" and "NNtag" stand for SECVTX $b$-tagging and NN $b$-tagging, respectively.

| Higgs mass ($\mathrm{GeV}/c^2$) | Expected signal events | | | |
|---|---|---|---|---|
| | Pretag | 1 tag | 1 tag with NNtag | $\geq 2$ tag |
| 110 | $4.81 \pm 0.34$ | $2.15 \pm 0.18$ | $1.87 \pm 0.18$ | $0.66 \pm 0.13$ |
| 115 | $3.99 \pm 0.28$ | $1.80 \pm 0.15$ | $1.56 \pm 0.15$ | $0.54 \pm 0.11$ |
| 120 | $3.23 \pm 0.23$ | $1.45 \pm 0.12$ | $1.26 \pm 0.12$ | $0.44 \pm 0.09$ |
| 130 | $2.05 \pm 0.15$ | $0.93 \pm 0.08$ | $0.81 \pm 0.08$ | $0.28 \pm 0.06$ |
| 140 | $1.03 \pm 0.07$ | $0.46 \pm 0.04$ | $0.40 \pm 0.04$ | $0.15 \pm 0.03$ |
| 150 | $0.40 \pm 0.03$ | $0.18 \pm 0.02$ | $0.16 \pm 0.02$ | $0.06 \pm 0.01$ |

TABLE VIII. Systematic uncertainties for various $b$-tagging requirements. The labels "tag" and "NNtag" refer to SECVTX and NN $b$-tagging, respectively.

| Source | uncertainty (%) | | |
|---|---|---|---|
| | 1 tag | 1 tag & NNtag | $\geq 2$ tag |
| Lepton ID | 2.0% | 2.0% | 2.0% |
| Trigger | <1% | <1% | <1% |
| ISR | 1.5% | 1.8% | 4.3% |
| FSR | 2.8% | 3.2% | 8.6% |
| PDF | 1.6% | 1.7% | 2.0% |
| JES | 2.3% | 2.3% | 3.0% |
| $b$-tagging | 3.8% | 5.3% | 16% |
| Total | 5.8% | 7.2% | 19% |

The systematic uncertainty on the SECVTX $b$-tagging efficiency is based on the scale factor uncertainty discussed in Sec. IV. When NN $b$-tagging is applied, the scale factor uncertainty is added to that of SECVTX in quadrature. The total systematic uncertainties for various $b$-tagging options are summarized in Table VIII.

## VII. OPTIMIZATION OF SEARCH STRATEGIES

The search strategy is optimized by calculating a signal significance defined as $S/\sqrt{B}$, where $S$ and $B$ are the number of expected signal and background events. In this analysis, $S$ and $B$ are counted within a window which gives the best significance in dijet mass distribution for the particular Higgs mass hypothesis being considered. The

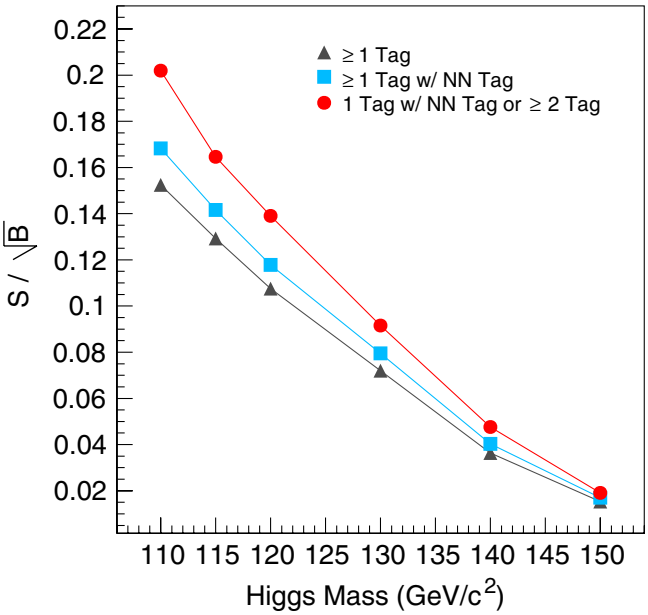


FIG. 6 (color online). Comparison of significance obtained from various $b$-tagging strategies. "Tag" and "NN Tag" represent SECVTX and NN $b$-tagging, respectively. The filled circles correspond to the combined analysis which treats disjoint samples with exactly one NN $b$-tag and two SECVTX tags separately.

window itself is optimized by varying the window peak and width for each $b$-tagging strategy. A comparison of the significance for various $b$-tagging options, shown in Fig. 6, provides an *a priori* metric that predicts which selection gives the best result.

Requiring the NN filter improves the sensitivity by about 10% in the sample of events with exactly one $b$ tag. The significance in double-tagged events is almost the same as that in events with at least one tag and no NN filter. Combining the two results therefore yields another sensitivity improvement. This combined use of two separate $b$-tagged samples provides a significant improvement as shown in Fig. 6. The total significance increases by 20% moving from "$\geq 1$ tag" to separate categories "1 tag $w$/NN tag" and "$\geq 2$ tag." Therefore, we quote final results from events having exactly one SECVTX $b$-tagged jet passing the neural network filter or at least two SECVTX $b$-tagged jets.

## VII. LIMIT ON HIGGS BOSON PRODUCTION RATE

As shown in Sec. VII, there is no significant excess number of events over the SM background expectation. Because the dijet mass resonance is a useful discriminant for the Higgs boson signature, we use a binned likelihood technique to fit the observed dijet mass distributions in Figs. 7 and 8, and set an upper limit on the $WH$ production cross section times $H \rightarrow b\bar{b}$ branching ratio.

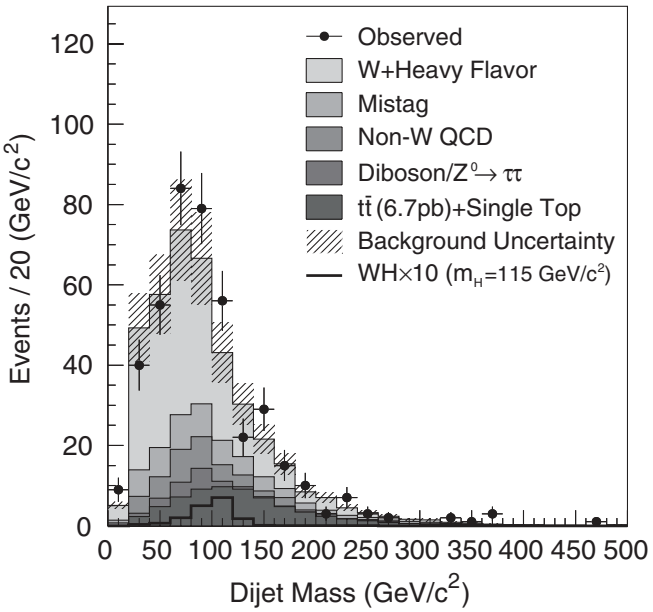


FIG. 7. Dijet mass distribution in $W + 2$ jets events including exactly one SECVTX $b$-tagged jet that passes the NN $b$-tagging filter. The contributions of the various background sources are shown in the histogram, while the hatched box on the background histogram represents the background uncertainty.

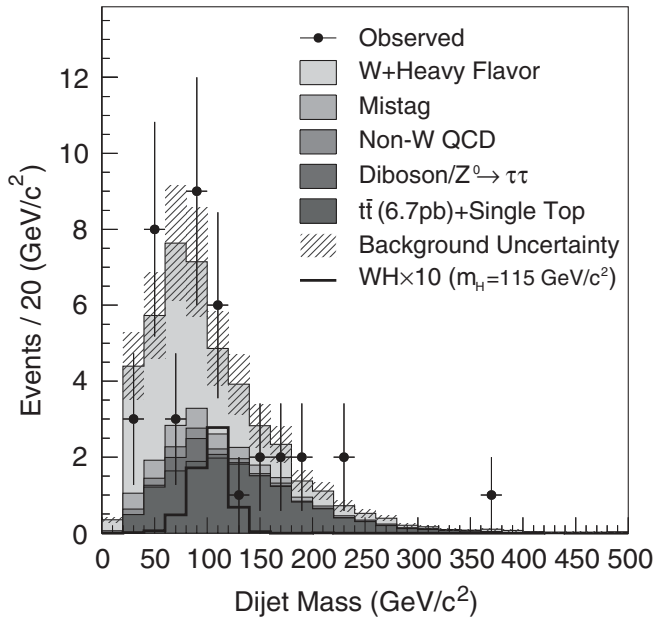


FIG. 8. Dijet mass distribution in $W + 2$ jets events including at least two SECVTX $b$-tagged jets.

### Binned likelihood technique

The number of events in each bin follows the Poisson distribution:

$$P_i(n_i, \mu_i) = \frac{\mu_i^{n_i} e^{-\mu_i}}{n_i!} (i = 1, 2, \ldots, N_{\text{bin}}) \qquad (11)$$

where $n_i$, $\mu_i$, and $N_{\text{bin}}$ represent the number of observed events in the $i$th bin, the expectation in the $i$th bin, and the total number of bins. The Higgs production hypothesis is constructed by setting $\mu_i$ to $\mu_i = s_i + b_i$, where $s_i$ and $b_i$ are the number of signal and expected background events in the $i$th bin. This quantity $s_i$ can also be written as a product:

$$s_i = \sigma(p\bar{p} \rightarrow W^{\pm}H) \cdot \mathcal{B}(H \rightarrow b\bar{b}) \cdot \epsilon_{WH} \cdot \int \mathcal{L} dt \cdot f_i^{WH}, \qquad (12)$$

where $\epsilon_{WH}$ is the signal efficiency described in Eq. (10) and $f_i^{WH}$ is the fraction of the total signal which lies in the $i$th bin. In this case, $\sigma(p\bar{p} \rightarrow W^{\pm}H) \cdot \mathcal{B}(H \rightarrow b\bar{b})$ is the variable to be extracted from data. An upper limit on the Higgs boson production cross section times branching ratio $\sigma(p\bar{p} \rightarrow W^{\pm}H) \cdot \mathcal{B}(H \rightarrow b\bar{b})$ is extracted by using a Bayesian procedure with a likelihood defined by

$$L = \prod_{i=1}^{N_{\text{bin}}} P_i(n_i, \mu_i) = \prod_{i=1}^{N_{\text{bin}}} \frac{\mu_i^{n_i} e^{-\mu_i}}{n_i!}. \qquad (13)$$

The background prediction $b_i$ includes contributions from the various background sources described in Sec. V:

$$b_i = N^{\text{TOP}} f_i^{\text{TOP}} + N^{\text{QCD}} f_i^{\text{QCD}}, \qquad (14)$$

where $f_i^{\mathrm{TOP}}$ and $f_i^{\mathrm{QCD}}$ are the fractions of the total number of top (including $t\bar{t}$ and single top) and QCD backgrounds (including $W$ + jets, non-$W$, and diboson) in mass bin $i$. There are systematic uncertainties in the estimates of both the number of signal events and the expected background. Such uncertainties modify the likelihood to be

$$L(\sigma\cdot\mathcal{B}) = \int_{N^{\mathrm{QCD}}}\int_{N^{\mathrm{TOP}}}\int_{N^{WH}}\prod_{i=1}^{N_{\mathrm{bin}}}\frac{\mu_i^{n_i}e^{-\mu_i}}{n_i!} \times G(N^{\mathrm{QCD}},\sigma^{\mathrm{QCD}})G(N^{\mathrm{TOP}},\sigma^{\mathrm{TOP}})G(N^{WH},\sigma^{WH}) \times dN^{\mathrm{QCD}}dN^{\mathrm{TOP}}dN^{WH}, \quad (15)$$

where the $G(N, \sigma)$ factors are truncated Gaussian densities constraints using the estimated numbers of events and the associated uncertainties. We assume a uniform prior for $\sigma\cdot\mathcal{B}$ and integrate the likelihood over all parameters except $\sigma\cdot\mathcal{B}$. A 95% C.L. upper limit on $\sigma\cdot\mathcal{B}$ is obtained by calculating the 95th percentile of the resulting distributions.

To measure the expected sensitivity for this analysis, background-only pseudoexperiments are used to calculate an expected limit in the absence of Higgs boson production. Pseudodata are generated by fluctuating the individual background estimates within total uncertainties. The expected limit is derived from the pseudodata using Eq. (15).

The likelihoods from events with exactly one SECVTX $b$-tagged jet passing the NN $b$-tagging filter and events with at least two SECVTX $b$-tagged jets criteria are multiplied together. The systematic uncertainties associated with the pretag acceptance, luminosity uncertainty, and uncertainty of the $b$-tagging efficiency scale factor are considered to be 100% correlated between the two selection channels. Background uncertainties, specifically on the heavy-flavor fractions and $b$-tagging scale factor, are also completely correlated. The "= 1 tag $w$/NN tag" selection combined with "≥ 2 tag" gives the best expected limit, as expected from the sensitivity study (see Fig. 6).

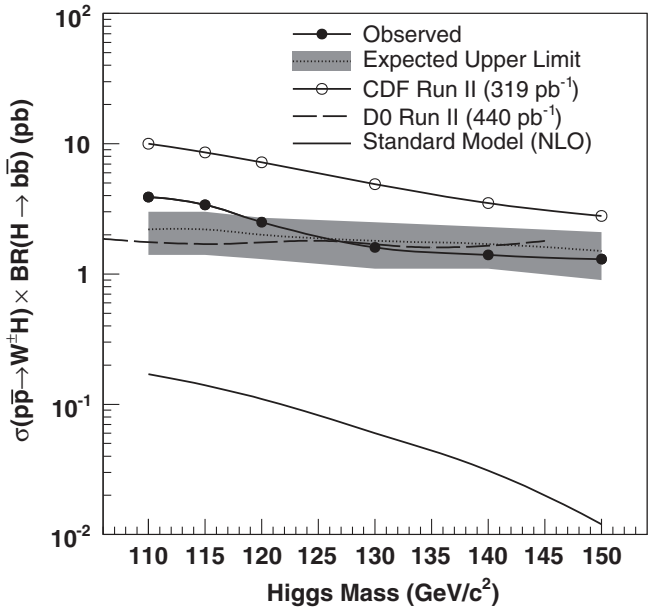


FIG. 9. 95% C.L. upper limit on $\sigma(p\bar{p}\rightarrow WH)\cdot\mathcal{B}(H\rightarrow b\bar{b})$ with an integrated luminosity of 1 fb$^{-1}$ obtained from the combined likelihood between events with exactly one SECVTX $b$-tag passing the NN $b$-tagging and events with at least two SECVTX $b$-tagged jets. The previous CDF data [7] and recent D0 data [8] are shown for comparison.

TABLE IX. Observed and expected upper limits on $\sigma(p\bar{p}\rightarrow WH)\cdot\mathcal{B}(H\rightarrow b\bar{b})$ at 95% C.L., compared to the SM production rate calculated at NLO.

| Higgs mass | Upper limit (pb) | | |
|---|---|---|---|
| GeV/$c^2$ | Observed | expected | SM |
| 110 | 3.9 | 2.2 ± 0.8 | 0.16 |
| 115 | 3.4 | 2.2 ± 0.8 | 0.13 |
| 120 | 2.5 | 2.0 ± 0.7 | 0.10 |
| 130 | 1.6 | 1.8 ± 0.7 | 0.060 |
| 140 | 1.4 | 1.7 ± 0.6 | 0.030 |
| 150 | 1.3 | 1.5 ± 0.6 | 0.011 |

The observed limits as a function of the Higgs boson mass are shown in Fig. 9 and Table IX, together with the expected limits determined from pseudoexperiments. An ensemble of limits from pseudoexperiments and the observed limit for each Higgs boson mass point are shown in Fig. 10. The limit in the low mass region is at most 2 standard deviations higher than the expected limit, but this is consistent with a statistical fluctuation in the dijet mass distributions (see Fig. 7) around $m_H = 115$ GeV/$c^2$. Such a fluctuation is much larger than the expectation for SM Higgs boson production in this channel.

The search sensitivity is improved significantly with respect to previous searches, about 30% beyond the expectations from simple luminosity scaling. The two main effects are the separation of the $b$-tagged data sample into single- and double-tagged events, and the NN filter applied to the single-tag sample.

## IX. CONCLUSIONS

We have presented a search for the standard model Higgs boson in the $\ell\nu b\bar{b}$ final state expected from $WH$ production. The event selection includes an additional neural network $b$-tag filter to reduce the background contributions from light-flavor and charm quark jets. This improvement, along with a total data set corresponding to 1 fb$^{-1}$, allows us to improve the upper limit on Higgs boson production. We set a 95% confidence level upper limit on the production cross section times branching ratio varying from 3.9 to 1.3 pb for Higgs boson masses 110 to 150 GeV/$c^2$.

## ACKNOWLEDGMENTS

We thank the Fermilab staff and the technical staffs of the participating institutions for their vital contributions.

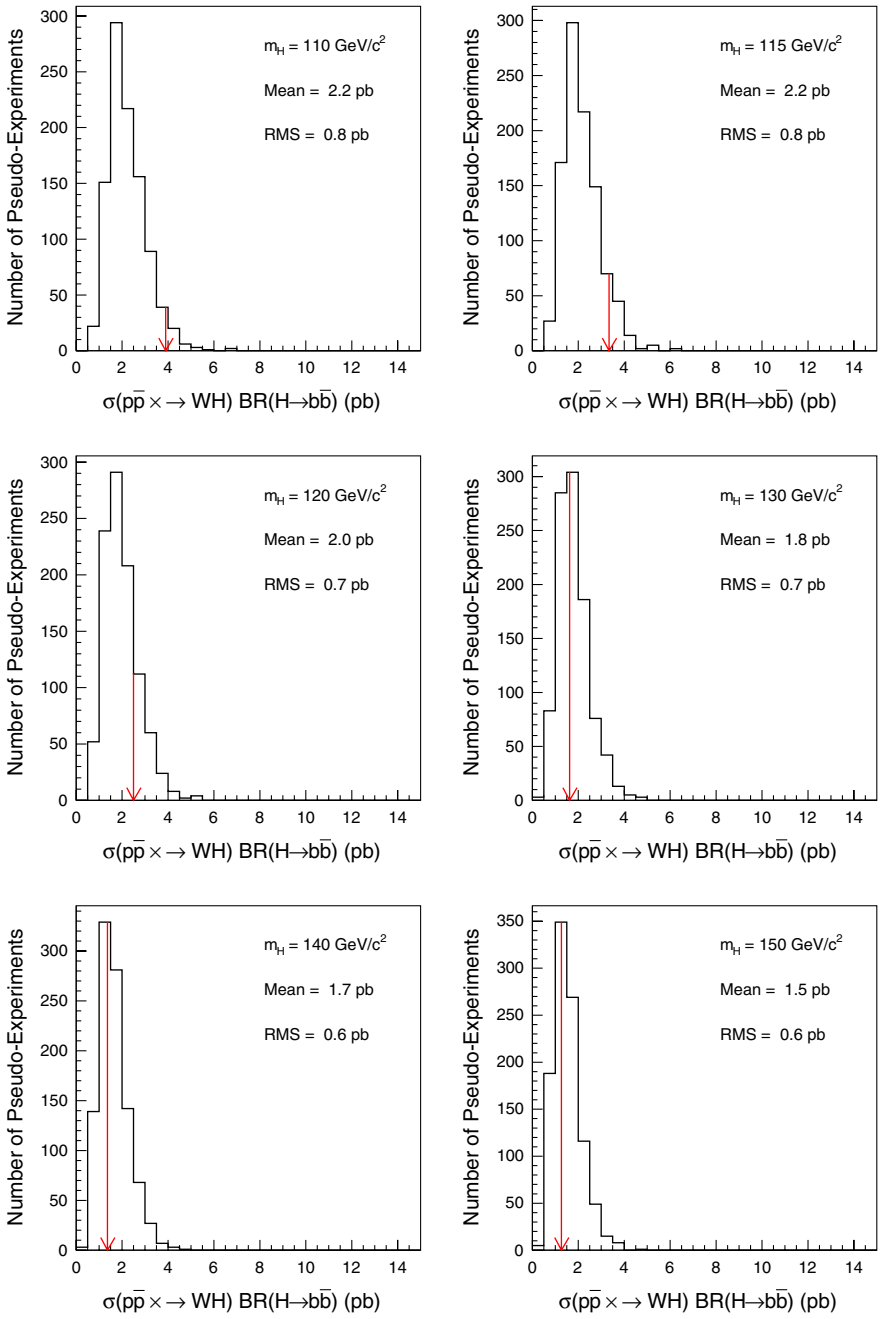


FIG. 10 (color online). Results of 95% C.L. limits obtained from the combined likelihood in pseudoexperiments. The arrows indicate the observed limits.

This work was supported by the U.S. Department of Energy and National Science Foundation; the Italian Istituto Nazionale di Fisica Nucleare; the Ministry of Education, Culture, Sports, Science and Technology of Japan; the Natural Sciences and Engineering Research Council of Canada; the National Science Council of the Republic of China; the Swiss National Science Foundation; the A.P. Sloan Foundation; the Bundesministerium für Bildung und Forschung, Germany; the Korean Science and Engineering Foundation and the Korean Research Foundation; the Science and Technology Facilities Council and the Royal Society, U.K.; the Institut National de Physique Nucleaire et Physique des Particules/CNRS; the Russian Foundation for Basic Research; the Comisión Interministerial de Ciencia y Tecnología, Spain; the European Community's Human Potential Programme; the Slovak R&D Agency; and the Academy of Finland.

[1] P. W. Higgs, Phys. Rev. Lett. **13**, 508 (1964).
[2] R. Barate *et al.* (ALEPH, DELPHI, L3, and OPAL Collaborations, and the LEP Working Group for Higgs boson searches), Phys. Lett. B **565**, 61 (2003).
[3] J. Alcaraz *et al.* (ALEPH, DELPHI, L3, and OPAL Collaborations, and the LEP Electroweak Working Group), Technical Report No. CERN-PH-EP-2006-042, 2006).
[4] T. Han and S. Willenbrock, Phys. Lett. B **273**, 167 (1991).
[5] A. Djouadi, J. Kalinowski, and M. Spira, Comput. Phys. Commun. **108**, 56 (1998).
[6] A. Abulencia *et al.* (CDF Collaboration), Phys. Rev. D **75**, 012010 (2007).
[7] A. Abulencia *et al.* (CDF Collaboration), Phys. Rev. Lett. **97**, 081802 (2006).
[8] V. M. Abazov *et al.* (D0 Collaboration), Phys. Lett. B **663**, 26 (2008).
[9] D. Acosta *et al.* (CDF Collaboration), Phys. Rev. D **71**, 052003 (2005).
[10] D. Acosta *et al.* (CDF Collaboration), Phys. Rev. D **71**, 032001 (2005).
[11] L. Balka *et al.*, Nucl. Instrum. Methods Phys. Res., Sect. A **267**, 272 (1988).
[12] S. Bertolucci *et al.*, Nucl. Instrum. Methods Phys. Res., Sect. A **267**, 301 (1988).
[13] M. G. Albrow *et al.*, Nucl. Instrum. Methods Phys. Res., Sect. A **480**, 524 (2002).
[14] F. Abe *et al.* (CDF Collaboration), Phys. Rev. D **45**, 1448 (1992).
[15] A. Bhatti *et al.*, Nucl. Instrum. Methods Phys. Res., Sect. A **566**, 375 (2006).
[16] G. Ascoli *et al.*, Nucl. Instrum. Methods Phys. Res., Sect. A **268**, 33 (1988).
[17] T. Dorigo (CDF Collaboration), Nucl. Instrum. Methods Phys. Res., Sect. A **461**, 560 (2001).
[18] E. J. Thomson *et al.*, IEEE Trans. Nucl. Sci. **49**, 1063 (2002).
[19] D. Acosta *et al.* (CDF Collaboration), Phys. Rev. Lett. **94**, 091803 (2005).
[20] A. Abulencia *et al.* (CDF Collaboration), Phys. Rev. Lett. **97**, 082004 (2006).
[21] C. Peterson, T. Rögnvaldsson, and L. Lönnblad, Comput. Phys. Commun. **81**, 185 (1994).
[22] A. Abulencia *et al.* (CDF Collaboration), Phys. Rev. D **74**, 072006 (2006).
[23] A. Abulencia *et al.* (CDF Collaboration), Phys. Rev. Lett. **97**, 082004 (2006).
[24] M. L. Mangano, M. Moretti, F. Piccinini, R. Pittau, and A. D. Polosa, J. High Energy Phys. 07 (2003) 001.
[25] G. Corcella *et al.*, arXiv:hep-ph/0201201.
[26] J. Campbell and R. K. Ellis, Phys. Rev. D **65**, 113007 (2002).
[27] M. Cacciari, S. Frixione, M. L. Mangano, P. Nason, and G. Ridolfi, J. High Energy Phys. 04 (2004) 068.
[28] B. W. Harris, E. Laenen, L. Phaf, Z. Sullivan, and S. Weinzierl, Phys. Rev. D **66**, 054024 (2002).
[29] T. Sjöstrand *et al.*, Comput. Phys. Commun. **135**, 238 (2001).
[30] A. Abulencia *et al.* (CDF Collaboration), Phys. Rev. D **73**, 032003 (2006).
[31] J. Pumplin *et al.*, J. High Energy Phys. 07 (2002) 012.